Supporting Information

A computational exploration of the crystal energy and charge carrier mobility landscapes of the chiral [6]helicene molecule

Beth Rice[1,2] *Luc M. LeBlanc,*[3] *Alberto Otero-de-la-Roza,*[4] *Matthew J. Fuchter,*[2,5] *Erin R. Johnson,*[3] *Jenny Nelson,* [1,2] *Kim E. Jelfs*[2,5]*

[1]Department of Physics, Imperial College London, South Kensington, London, SW7 2AZ, U. K.

[2]Centre for Plastic Electronics, Imperial College London, South Kensington, London, SW7 2AZ, U. K.

[3]Department of Chemistry, Dalhousie University, Halifax, Nova Scotia, B3H 4R2, Canada.

[4]Department of Chemistry, University of British Columbia, Okanagan, 3247 University Way, Kelowna, British Columbia, V1V 1V7, Canada.

[5]Department of Chemistry, Imperial College London, South Kensington, London, SW7 2AZ, U. K.

Email: k.jelfs@imperial.ac.uk

1. Additional methodological details

1.1. Crystal Structure Prediction (CSP)

A molecular model of [6]helicene was constructed manually and geometry optimised in Gaussian09[1] at the B3LYP/6-31G(*d,p*) level of theory. CrystalPredictor[2,3] was used to generate the hypothetical crystal structures, with the search restricted to structures with a single molecule in the asymmetric unit ($Z'=1$) and using only common space groups that included both enantiopure and racemic packings; $P1$, $P2_1$, $P2_12_12_1$, $P2_12_12$, $P4_12_12$, $R3$, $C2$, $C222_1$, $P2_1/c$, $P\bar{1}$, $C2/c$, $Pbca$, $Pna2_1$, $Pnma$, $Pca2_1$, $Pbcn$, Pc, Cm, $Cmc2_1$, $Aba2$, $Fdd2$, $Iba2$, $Pnna$, $Pccn$, $Pbcm$, $Pnnm$, $Pmmn$, $Cmcm$, $Cmca$, $Fddd$, $Ibam$, $Pa\bar{3}$, $P2_1/m$, $C2/m$, $P2/c$, $P4/n$, $P4_2/n$, $I4/m$, $I4_1/a$, $R3c$, $R\bar{3}c$, $P6_3/m$, $P\bar{4}2_1c$, $I\bar{4}2d$, $I\bar{4}$, Cc, $P4_1$, $P4_3$, $P4_12_12$, $P4_32_12$, $P3_1$, $P3_2$, $P\bar{3}$, $R\bar{3}$, $P3_121$, $P3_221$, $P6_1$, $P6_3$ and $P2_13$.

The structure search was conducted with the helicene treated as a rigid molecule, with the electrostatic component of the intermolecular forces evaluated based upon a distributed multipole analysis[4] (calculated using GDMA2)[5] of the molecular charge density computed at the MP2/6-31G(*d,p*) level of theory. This model has been shown to provide good accuracy for - interactions in systems, such as [6]helicene, containing -electron density.[6] The remaining intermolecular forces were calculated using the Williams potential,[7] which provides a good description for hydrocarbon molecules. Approximately 500,000 structures were tested, at which point no new structures were found with additional steps. The unique structures from the search (~10,000) were then lattice energy minimised using DMACRYS,[6] with second derivatives being calculated to confirm the structures to be true minima.

As there were reports of enantiomeric intergrowths for [6]helicene,[8] we constructed three intergrowth models manually, as these would not be found in the restricted search described above. These three intergrowth models (see Fig. S1) vary by the translation of the opposite enantiomers along the interface by 0, ½, or ¼ of the unit cell, and match those previously considered by Thomas *et al.*.[8] The lowest energy stable structure was that previously found by Thomas *et al.* to be the most stable based upon computed surface energies,[8] and corresponds to no translation of the unit cell along the interface. This intergrowth structure has (100) interfaces between enantiomeric regions. We generated this intergrowth model by taking the unit cell of the experimentally reported [6]helicene structure (Cambridge Crystallographic Database Centre (CCDC) code HEXHEL) and firstly doubling the cell along the *b* axis, so that it contained 8 molecules. We created an inverted form of this cell and displaced these molecules to form the interface between left- and right-handed molecules. This structure was energy minimised as described above with the Williams potential (W99) in DMACRYS. Fig. 2 shows the intergrowth structure and how this relates to the enantiopure HEXHEL structure.

1.2. DFT optimisation of low energy structures from CSP

The geometry relaxations were carried out with tight convergence criteria (10^{-5} Ry energy threshold). For the electronic steps, a 2x2x2 k-point grid and cutoff energies of 60 Ry for the plane-wave expansion and 600 Ry for the density expansion were used. The parameters for the XDM damping function were a1=0.6512 and a2=1.4633 Å. The energy of the isolated molecule, necessary for calculation of the lattice energies, was computed using a cubic supercell with side lengths of 50 Bohr. The DFT optimized structures are provided as supporting information to this article.

1.3. Crystal structure comparisons

Crystal structure comparisons were performed using the COMPACK[9] procedure in Mercury,[10] with clusters of 15 molecules compared and their root mean square deviation ($RMSD_{15}$) calculated for the positions of the carbon atoms only. A packing similarity tree diagram was constructed with a procedure similar to that reported previously,[11] with similarity searches between the 27 low energy structures determined for clusters of 2, 3, 4, 6, 8, 12 and 15 molecules. This uncovered ten substructure features that were found in multiple crystal structures. These features were searched for across the structures; the reference crystal structure used to search for each feature is given in Table S1. The geometric similarity tolerances used for the searches were distances within 30% and angles within 20 degree. Matches were only retained when the root mean square (RMS) difference was below 0.5 Å. Molecular structures of each of these substructures are provided as supporting information to this article.

1.4. Charge mobility calculations

The Marcus equation gives the rate of charge hopping from molecule *i* to *j* as:[12]

$$\Gamma_{ij} = \frac{|J_{ij}|^2}{\hbar}\sqrt{\frac{\pi}{\lambda k_B T}}\,exp\left(\frac{-(\Delta E_{ij}+\lambda)^2}{4\lambda k_B T}\right)$$

where J_{ij} is the transfer integral and ΔE_{ij} is the change in energy between sites *i* and *j*, and λ is the reorganisation energy. The reorganisation energy is the energy cost associated with the rearrangement of the molecules involved in the hop and their surroundings. The reorganisation energy is a sum of the inner (λ_i) and outer (λ_0) reorganisation energies, which refer to the molecules and their surroundings respectively. The inner reorganisation energy was calculated with the 4-point method:[13]

$$\lambda_i = E^+_{neutral} - E^+_{charged} + E^0_{neutral} - E^0_{charged}$$

where E^+ and E^0 are the total energies of the charged and neutral molecules respectively, and *neutral* and *charged* indicate that the energy is computed in the ground state geometry of the neutral or charged molecule. The inner reorganisation energy was calculated to be 0.16 eV and since the outer reorganisation energy is more difficult to quantify, it was approximated as 0.3 eV. A condition for the Marcus equation to be valid is that $J << \lambda$ and as long as this is true, then λ will just act as a scaling factor. For all structures studied, the maximum transfer integral was less than 0.1 eV.

The change in energy between the sites is:

$$\Delta E_{ij} = \varepsilon_i - \varepsilon_j - q\vec{F}.\vec{r}_{ij}$$

where ε_i and ε_j are the energies of sites i and j respectively, q is the charge on an electron, $\vec{F}$ is the field vector and $\vec{r}$ is the distance vector between sites i and j. It is taken as zero when there is no field present, *i.e.* no energetic disorder is included in the model. The angular dependent mobility was found with this method by applying a field of strength 10000 V cm^{-1} at 10 degree intervals in each of the 3 planes. To get a mobility from the set of rates, a Master equation[14] was constructed according to:

$$\frac{dP_j}{dt} = \sum_{i \neq j} \left[\Gamma_{ij} P_i(t) - \Gamma_{ji} P_j(t)\right]$$

where P_j is the probability of site j being occupied by a charge and Γ_{ij} is the rate of hopping between sites i and j. The equation is valid in the low charge limit. By considering a matrix A defined as:

$$A_{ij} = \begin{cases} \Gamma_{ij}, i \neq j \\ -\sum_{i \neq j} \Gamma_{ij}, i = j \end{cases}$$

The master equation can be solved in steady state with $AP = 0$. The steady state probabilities can then be used to find the average velocity of charges with

$$\vec{v} = \sum_{i \neq j} \overrightarrow{r_{ij}} A_{ij} P_j$$

and finally the mobility with

$$\mu = \frac{\langle v \rangle}{F}$$

where $\langle v \rangle$ is the average velocity of the charges in the direction of the field and F is the magnitude of the field.

1.5. Generation of two-dimensional fingerprint plots

The two-dimensional (2D) fingerprint plots of the Hirshfeld surface were generated using standard documented procedures with Crystal Explorer 3.1.[15-18]

2. Additional discussion of [6]helicene CSP results

2.1. Context of [6]helicene results within carbohelicene family

Other unfunctionalised carbohelicenes have also been reported in the chiral $P2_12_12_1$ space group, including [4]helicene (benzo(c)phenanthrene, CCDC code BZPHAN),[19] which Kitaigorodsky proposed was the preference for organic molecules with a C_2 symmetry element.[20] For larger helicenes, including [7]helicene (HPTHEL),[21] [10]helicene (THELIC)[22] and [11]helicene (UHELIC),[22] their enantiopure crystal structures have been reported in the monoclinic $P2_1$ space group. The second lowest energy enantiopure predicted crystal structure (**8**) was found to lie 2.8 kJ mol^{-1} above **1**, although still exhibiting the common substructure features as for **1**, **2** and **3**, but with weaker intermolecular interactions (Fig. S6). [4]helicene has not been reported to form a racemate crystal structure, as it spontaneously resolves into a conglomerate of enantiopure crystals, based on computed small thermodynamic preferences (0.3 kJ mol^{-1}).[23] For [5]helicene there are two reported racemic crystal structures: Form A in a $P2_1/c$ space group and Form B in a A2/a space group (DBPHEN02 and DBPHEN03).[20] For [7]helicene, racemate crystal structures in both $P2_1/n$ and $P2_1/c$ (HPTHEL01 and HPTHEL03) space groups have been reported,[21] although conglomerates of enantiopure crystals in solution can also form.[24] For larger helicenes, we could not find reports of racemate crystal structures in the CCDC. The historical reports of unfunctionalised carbohelicene crystal structures combined with our CSP results for [6]helicene suggest a couple of notions; as is typical for many organic molecules, there are very small energetic differences between the lowest energy enantiopure and racemate crystal structures for the carbohelicenes. These energetic differences, and therefore preferences for *e.g.* spontaneous resolution, are extremely sensitive to small

changes in packing and the ability to maximise non-covalent interactions. Therefore preference for spontaneous resolution or racemate formation change continuously with helicene size and, by extension, with any added functionality to the helicene. This demonstrates the utility of using CSP to predict the packing (and then properties) as part of the design process for a new helicene molecule, as the packing of the helicenes is too sensitive for chemical intuition alone to be reliable.

2.2. Investigation of structure differences at a molecular level in the [6]helicene CSP results

We have also investigated differences in the molecular structures of the helicenes across our lattice energy landscape, including comparing the angles between planes of the aromatic rings (according to Martin[25]). We found no significant differences or interesting trends across our predicted structures. Of most interest was the "opening angle" (3) of the [6]helicene, which can be described as the most characteristic shape descriptor for these molecules, the results are shown in Fig. S5. The range of this opening angle was 39-48°, with only minor distortions compared to the value of 43.6° in the gas phase structure (MP2/6-31G(*d,p*)). Compared to functionalised [6]helicenes, where the opening angle has been reported with a range of 20-52°, the variations in the predicted carbo[6]helicene are small.[20] The smallest opening angle of 39° was found for the enantiopure structure **8**, which fits with previous reports that chiral space groups often result in less "open" helicenes.[20]

3. Supplementary tables and figures

Table S1: The substructure features contained within each of the energetically low-lying crystal structures. A filled box indicates the substructure is found in that crystal structure, with colouring as per Figure 5 in the main paper. The reference crystal structure used for each search is marked "Ref", with the number of molecules used in the search given in brackets.

Crystal structure	Homochiral interlocked pair (**IV**)	Heterochiral interlocked pair (**III**)	Homochiral back-to-back pair (**II**)	Heterochiral back-to-back pair; edge (**VII**)	Heterochiral back-to-back pair; centre (**VI**)	Homochiral chain (**V**)	Interlocked heterochiral chain (**VIII**)	Adjacent heterochiral chain (**IX**)	Adjacent translational homochiral chain (**I**)	Herringbone tramslational homochiral chain (**X**)
1	Ref (2)								Ref (4)	
2										
3										
4										
5										
6										
7										
8						Ref (4)				
9										
10										
11										
12					Ref (2)					
13										
14										
15										
16								Ref (4)		Ref (4)
17										
18										
19										
20										
21		Ref (2)	Ref (2)	Ref (2)			Ref (4)			
22										
23										
24										
25										
26										
27										

Table S2: A comparison of relative energies and density for the crystal structures that were found to be lowest in energy after the rigid-molecule search and for the intergrowth structure. The cells for the intergrowth structure are coloured red, those for enantiopure structures blue, while those for racemic structures are left uncoloured.

DFT ranking	DFT relative energy (kJ mol^{-1})	Rigid molecule, W99 relative energy (kJ mol^{-1})	Density after DFT relaxation (g cm^{-3})	Space group
1 (HEXHEL)	0.00	0.85	1.362	P212121
2	0.60	2.29	1.363	P1 (Z'=8)
3	0.80	4.19	1.358	Pna21
4	1.11	0.00	1.353	P21/c
5	2.02	11.29	1.375	P21/c
6	2.56	10.19	1.379	P-1
7	2.69	7.02	1.362	P21/c
8	2.75	9.51	1.351	P21
9	4.45	8.79	1.347	P21/c
10	4.55	9.72	1.336	P21/c
11	4.61	9.22	1.337	P21/c
12	4.72	11.21	1.348	P21/c
13	5.06	12.17	1.348	P21/c
14	5.26	11.95	1.334	P212121
15	5.59	10.70	1.330	Cc
16	5.78	5.82	1.368	PBCN
17	6.12	11.99	1.337	P21/c
18	6.33	11.99	1.325	Pbca
19	6.48	12.05	1.338	C2/c
20	6.52	11.63	1.357	P21/c
21	6.71	10.58	1.338	P21/c
22	6.92	13.01	1.304	C2
23	6.94	12.54	1.306	Pca21
24	7.02	13.14	1.340	P21/c
25	7.10	8.25	1.341	Pbca
26	7.11	12.22	1.357	P-1
27	7.19	12.15	1.327	P21/c
28	7.29	12.96	1.307	Pbca
29	7.49	13.01	1.302	P21212
30	7.49	13.07	1.302	P21212
31	7.73	12.92	1.330	P-1
32	7.75	12.91	1.330	P-1
33	7.92	13.02	1.313	P21/c
34	8.48	13.15	1.333	P-1
35	8.50	13.11	1.333	P-1
36	8.68	13.06	1.333	P-1
37	9.33	10.41	1.300	Pbca

38	9.34	12.68	1.324	P21/c
39	10.27	6.75	1.301	Pbca
40	10.90	12.86	1.287	C2/c
41	11.00	12.92	1.287	C2/c
42	11.32	9.03	1.331	Pbca
43	11.89	12.94	1.289	C2/c
44	11.96	11.71	1.283	Pna21
45	12.28	12.44	1.302	P21/c
46	12.61	11.25	1.327	P-1
47	13.92	9.89	1.283	Pbca
48	15.14	12.94	1.314	P21/c
49	15.42	12.41	1.276	P21/c

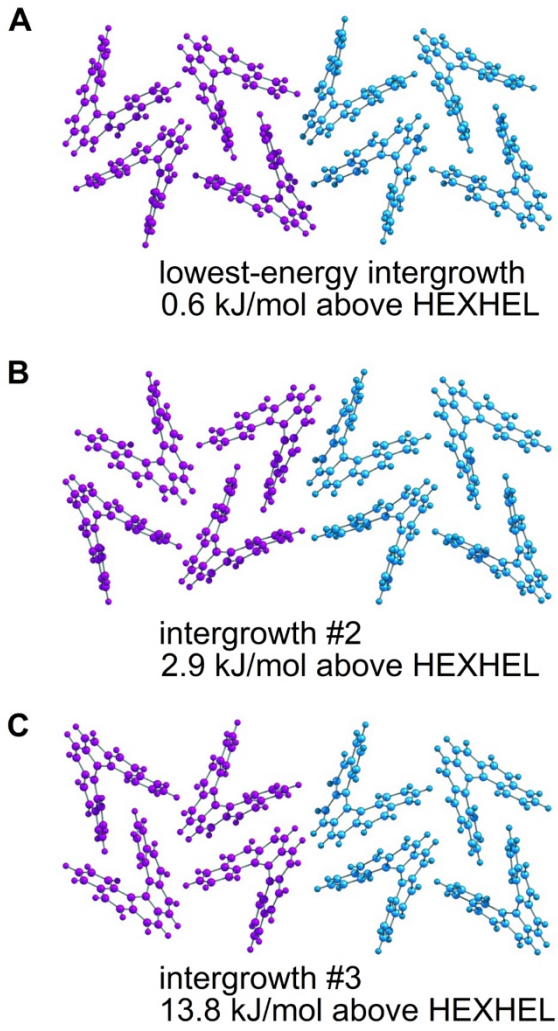

*Figure S1: The three alternative integrowth models that were considered, with their relative energy compared to structure **1** (HEXHEL) given. Opposite enantiomers are shown in purple and cyan.*

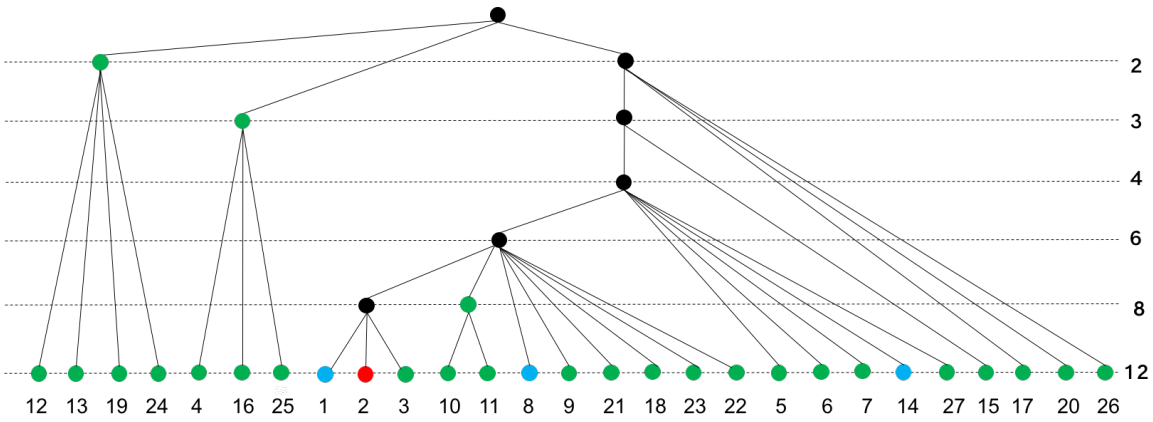

Figure S2: A packing similarity diagram for the energetically low-lying [6]helicene polymorphs. Each vertical level corresponds to the number molecules in a cluster found to be similar, as labelled on the right. Points in green are for racemates, in blue for enantiopure structures, and in red for the intergrowth.

Table S3: A summary of packing similarity features found for each node in the packing similarity tree diagram.

Structures	Packing similarity feature(s)	No. of molecules in cluster
1, 2, 3	• Homochiral chains of molecules with alternating interlocking and back-to-back helicenes. • Homochiral columns formed by translational symmetry.	8
10, 11	• Heterochiral interlocked pair. • Homochiral back-to-back pair. • Homochiral columns formed by translational symmetry.	8
1, 2, 3, 10, 11, 8, 9, 21, 18, 23, 22	• Homochiral back-to-back pairs. • Homochiral columns formed by translational symmetry.	6
1, 2, 3, 10, 11, 8, 9, 21, 18, 23, 22, 5, 6, 7, 14, 27	Homochiral columns formed by translational symmetry.	4
1, 2, 3, 10, 11, 8, 9, 21, 18, 23, 22, 5, 6, 7, 14, 27	Homochiral columns formed by translational symmetry.	3
4, 16, 25	Heterochiral cluster	3
12, 13, 19, 24	Heterochiral back-to-back pair	2

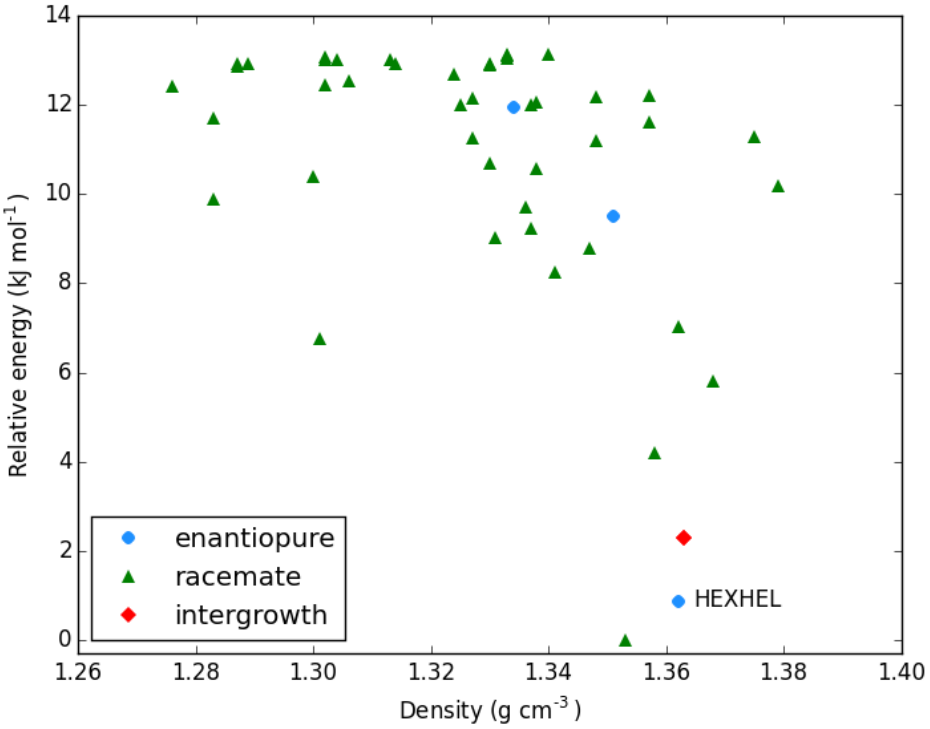

Figure S3: Lattice energy landscape for the rigid-body search with the W99 potential. The structure labelled HEXHEL is the observed enantiopure structure.

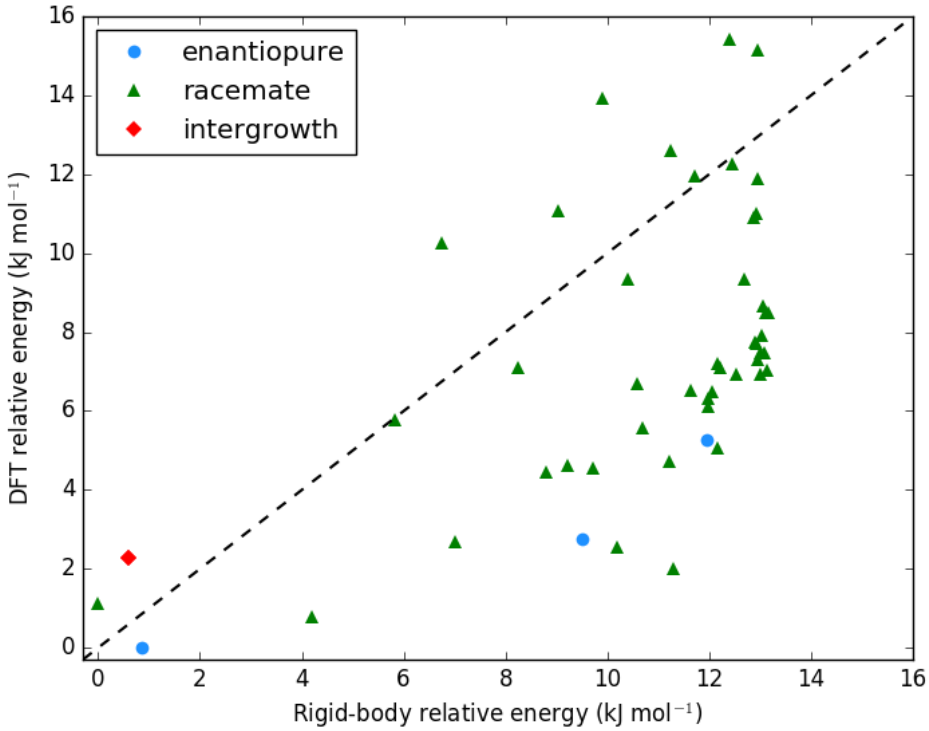

Figure S4: Comparison of the relative energies determined from the rigid-body search with the W99 potential to those when the structures are relaxed with the B86bPBE-XDM method. The dashed line corresponds to a perfect match between the methods.

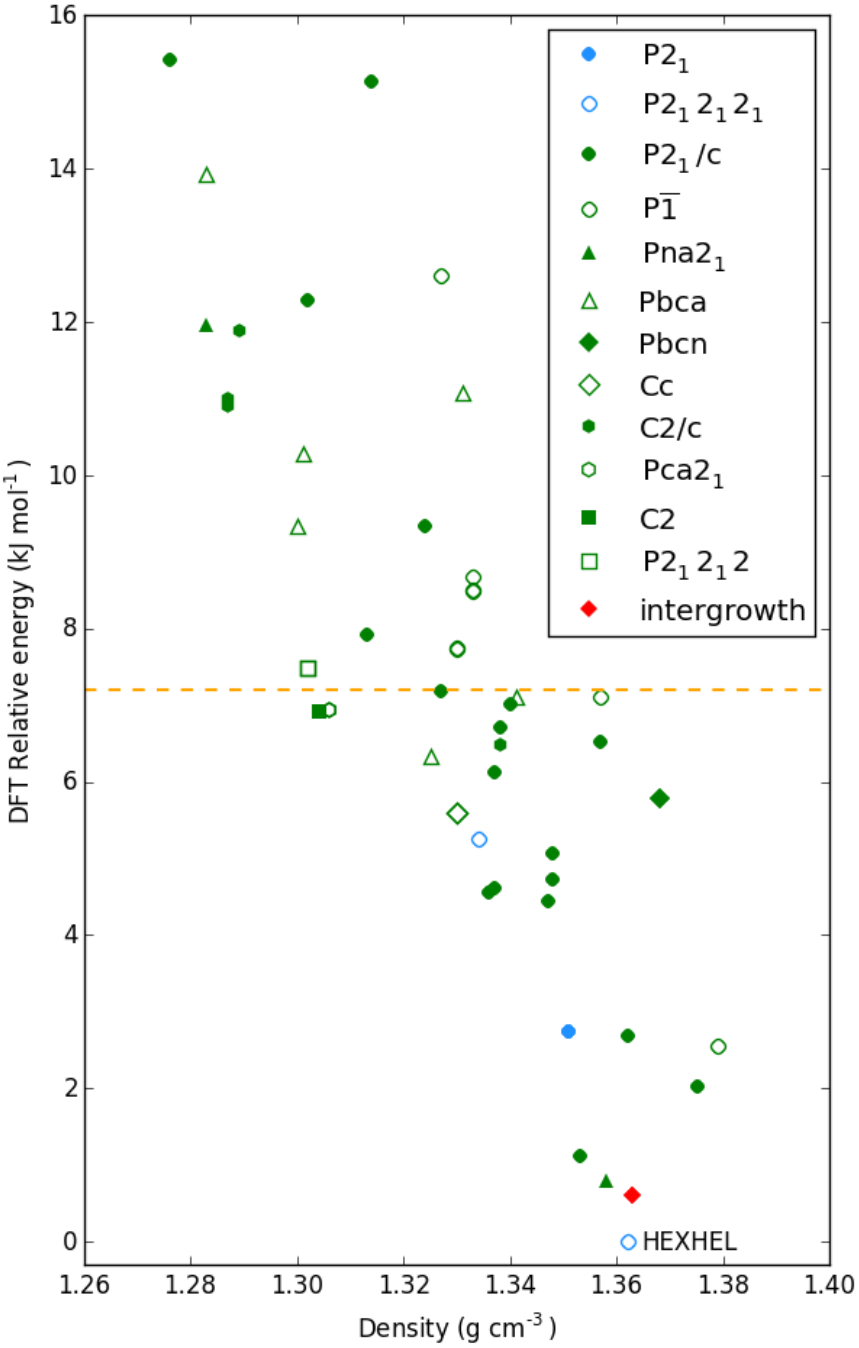

Figure S5: Lattice energy landscape with the B86bPBE-XDM method for [6]helicene, with structures labelled according to their space group. Enantiopure structures are labelled in blue, racemates in green, and the intergrowth in red. The structure labelled HEXHEL is the observed enantiopure structure.

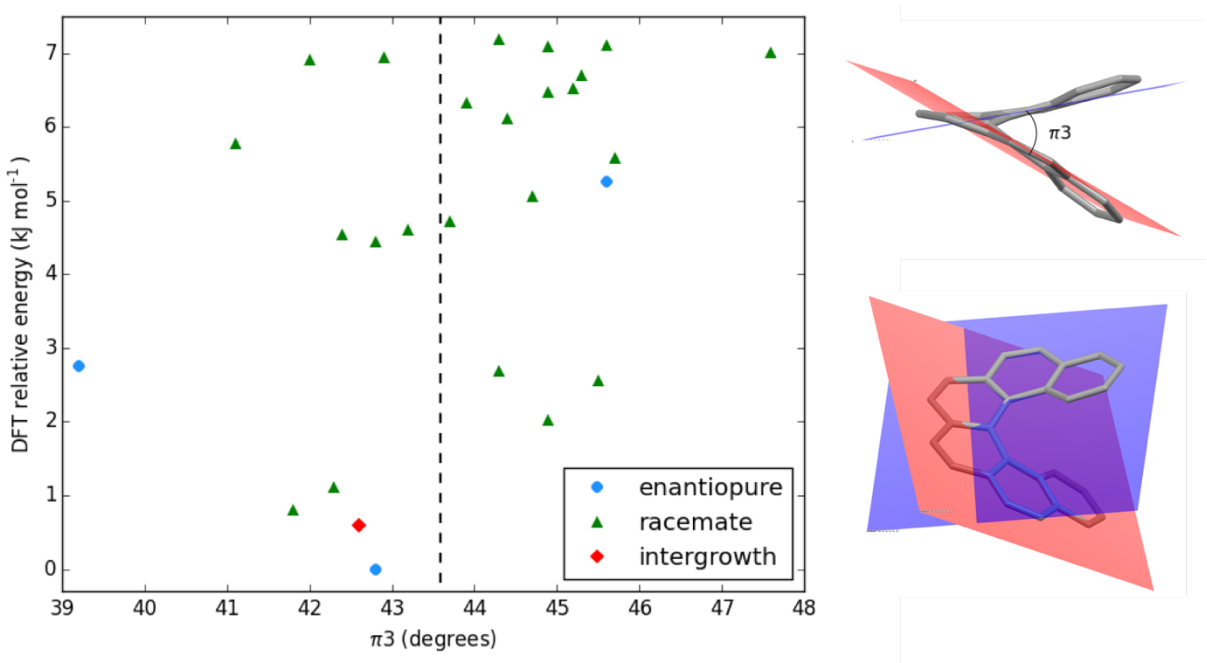

Figure S6: (left) The "opening angle", 3, of the [6]helicene molecules in the low-lying polymorphs compared to their relative B86bPBE-XDM energies. The dashed line shows the angle for the isolated molecule calculated at the B3LYP/6-31G(d,p) level of theory; (right) the [6]helicene molecule shown from two alternative perspectives. The 3 angle is calculated by measuring the angle between the two planes (here shown in red and blue) formed by the second and fifth aromatic rings in the molecule, as defined by Martin.[25]

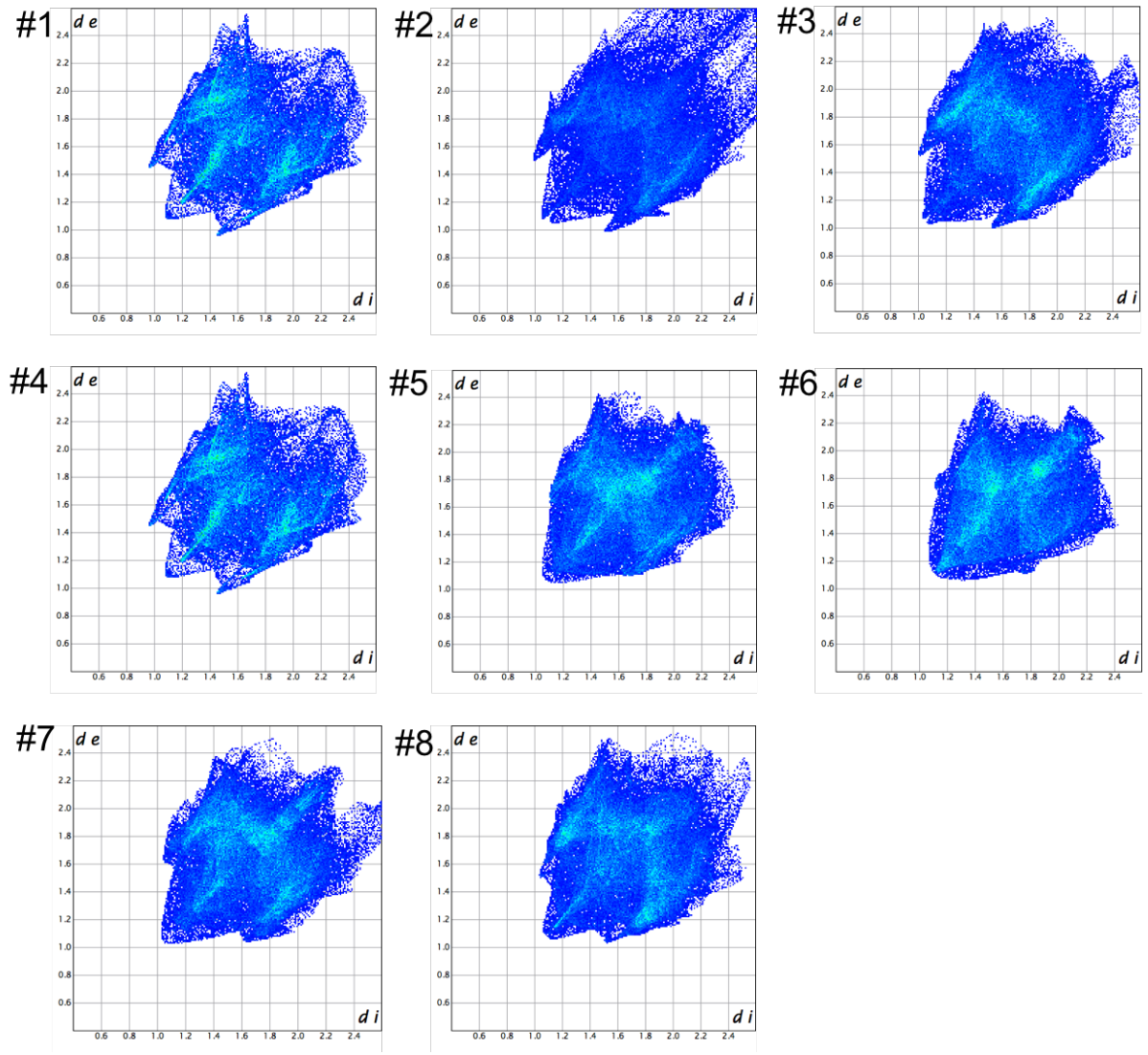

*Figure S7: Two-dimensional (2D) fingerprint plots for the eight lowest lying crystal structures for [6]helicene. All plots were generated showing the region between 0.4 – 2.5 Å only. The distance to the external surface, d_e, on the y-axis measures the distance from the helicene molecule's surface to the nearest atom on a neighbouring molecule. The distance to the internal surface, d_i, is the distance from the helicene molecule's surface to the nearest atom on the same molecule. Royal blue corresponds to a low frequency occurrence of a (d_i, d_e) pair, while brighter spots indicate relatively higher frequency of a (d_i, d_e) combination at a molecular surface point. π-π interactions between aromatic rings would show as brighter spots on the diagonal at ~1.7-1.8 Å, whilst C-H---π interactions would show as "wings" on the structure (as found in all but structures ranked **5** and **6** here).*

Table S4: A comparison of hole mobilities in the low energy structures. The anisotropy is defined in two ways: as the normalised standard deviation of the angular dependent mobility, and as the ratio between the maximum and minimum mobility. The cells for the intergrowth structure are coloured red, those for enantiopure structures blue, and those for racemic structures are left uncoloured.

DFT ranking	Maximum hole mobility ($cm^2\ V^{-1}\ s^{-1}$)	Maximum hole transfer integral, *J* (eV)	Anisotropy for hole mobility (normalised standard deviation)	Anisotropy for hole mobility (ratio of maximum/ minimum)
1 (HEXHEL)	0.73	0.03	0.26	5.4
2	0.74	0.03	0.26	7.2
3	0.92	0.03	0.25	176.0
4	2.00	0.06	0.27	157.3
5	0.15	0.03	0.29	9.1
6	0.74	0.06	0.31	39.5
7	0.71	0.03	0.31	35.9
8	0.02	0.02	0.19	3.0
9	0.11	0.02	0.20	2.9
10	0.01	0.03	0.32	9.0
11	0.41	0.03	0.30	12.0
12	0.00	0.07	0.30	109.4
13	1.26	0.11	0.29	7.8
14	0.46	0.02	0.28	8.9
15	0.35	0.03	0.31	9.7
16	1.68	0.06	0.36	45.4
17	0.40	0.17	0.33	22.7
18	0.27	0.07	0.26	21.3
19	1.09	0.07	0.22	11.8
20	0.53	0.06	0.15	2.6
21	0.53	0.36	0.35	27.4
22	0.14	0.02	0.28	13.2
23	0.01	0.02	0.24	7.2
24	1.32	0.10	0.25	4.7
25	1.23	0.10	0.34	18.5
26	0.01	0.05	0.23	4.4
27	0.14	0.02	0.23	5.7

Table S5: A comparison of electron mobilities in the low energy structures. The anisotropy is defined in two ways: as the normalised standard deviation of the angular dependent mobility, and as the ratio between the maximum and minimum mobility. The cells for the intergrowth structure are coloured red, those for enantiopure structures blue, and those for racemic structures are left uncoloured.

DFT ranking	Maximum electron mobility ($cm^2 V^{-1} s^{-1}$)	Maximum electron transfer integral, J (eV)	Anisotropy for electron mobility (normalised standard deviation)	Anisotropy for electron mobility (ratio of maximum/ minimum)
1 (HEXHEL)	2.15	0.06	0.29	21.1
2	1.89	0.07	0.28	7.4
3	2.24	0.07	0.37	739.1
4	0.80	0.03	0.27	39.5
5	1.67	0.06	0.27	12.8
6	1.14	0.06	0.28	8.1
7	1.55	0.06	0.29	10.3
8	1.60	0.07	0.31	23.5
9	1.64	0.06	0.27	5.5
10	2.37	0.07	0.31	43.2
11	2.90	0.07	0.32	38.3
12	0.64	0.06	0.31	15.8
13	1.55	0.17	0.29	12.0
14	1.05	0.05	0.35	36.8
15	2.00	0.07	0.36	30.5
16	0.61	0.03	0.29	5.3
17	0.14	0.25	0.18	2.3
18	1.88	0.13	0.31	19.7
19	0.33	0.11	0.27	9.5
20	0.82	0.08	0.24	4.1
21	2.66	0.21	0.30	22.8
22	1.50	0.07	0.36	6.1
23	0.85	0.06	0.24	8.0
24	0.60	0.10	0.24	4.9
25	0.59	0.10	0.25	6.0
26	2.35	0.12	0.28	7.9
27	0.95	0.05	0.28	5.6

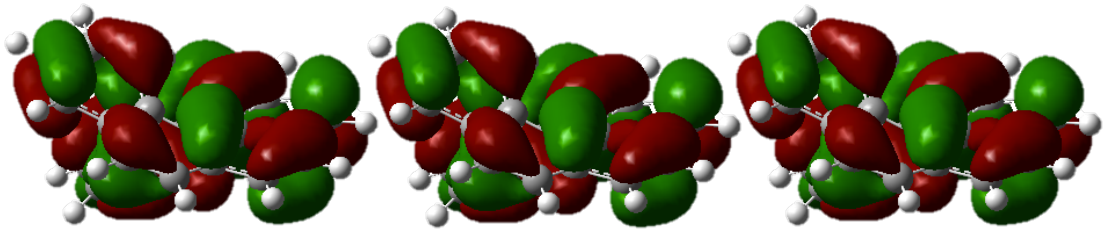

(a)

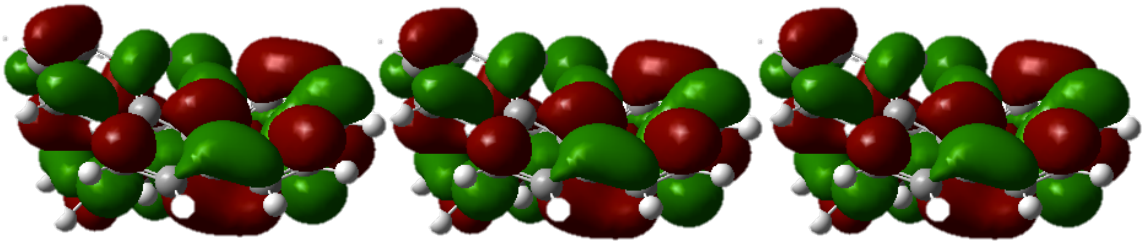

(b)

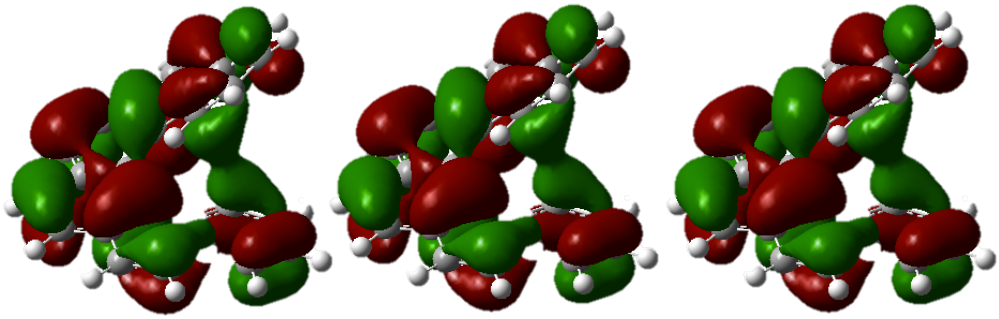

(c)

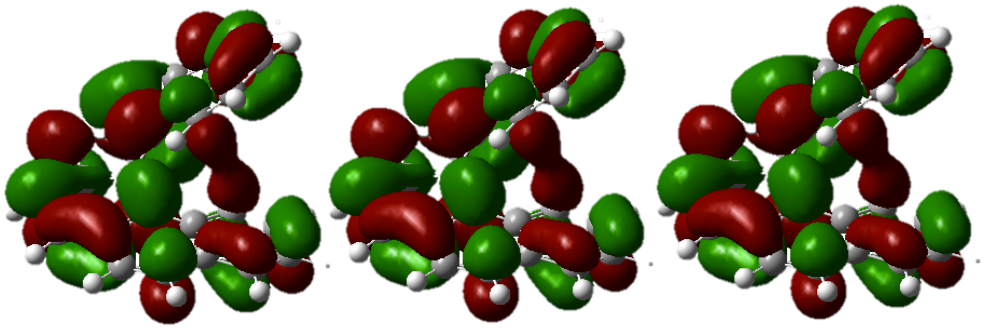

(d)

Figure S8: (a) HOMO and (b) LUMO orbitals showing the high hole mobility pathway along the herringbone translational homochiral chain in structure ***4****. (c) HOMO and (d) LUMO orbitals showing the high electron mobility pathway along the adjacent translational homochiral chain in structure* ***11****.*

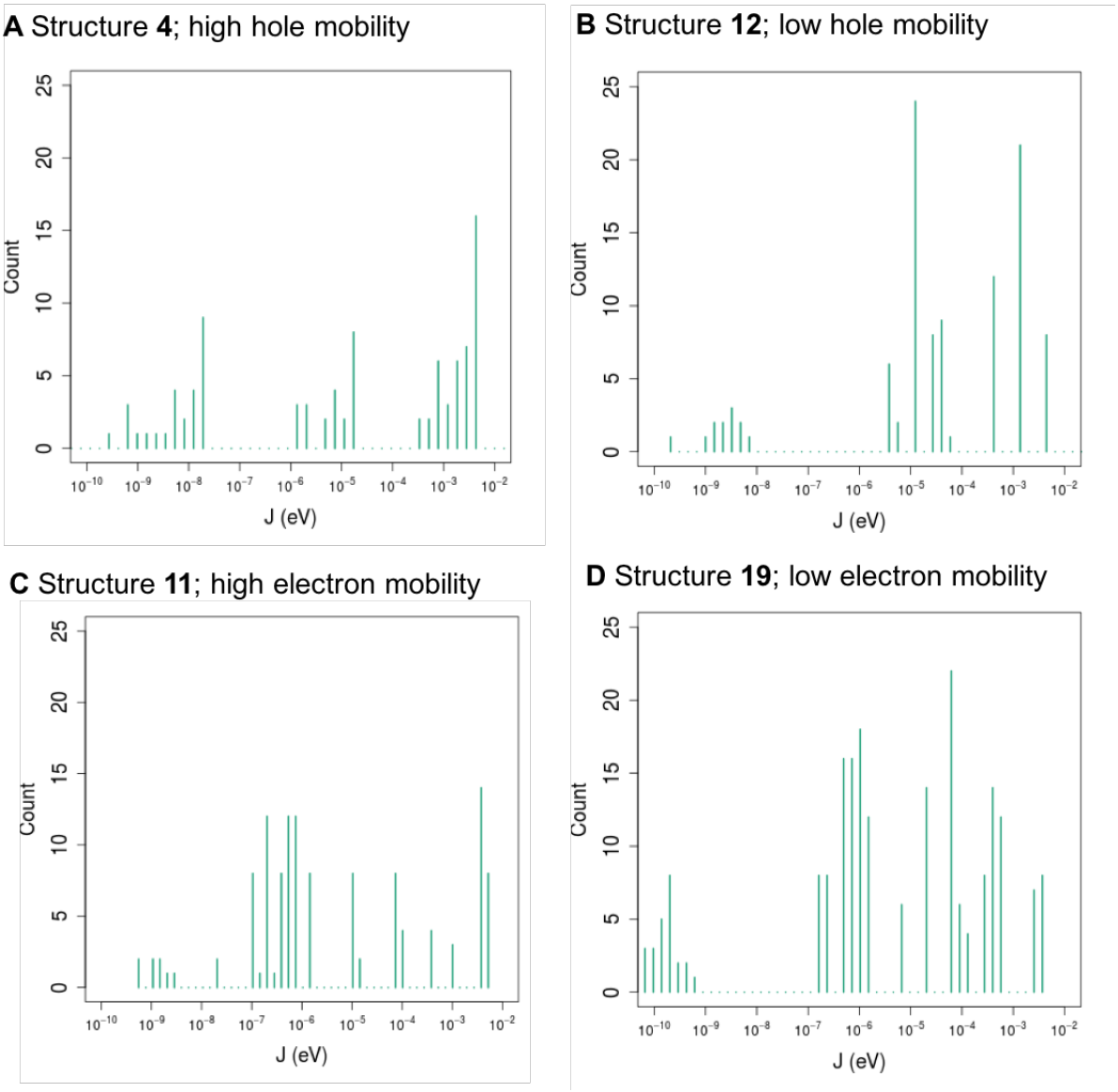

Figure S9: Histograms comparing the complete set of transfer integrals (J) for the highest and lowest charge carrier mobility [6]helicene structures.

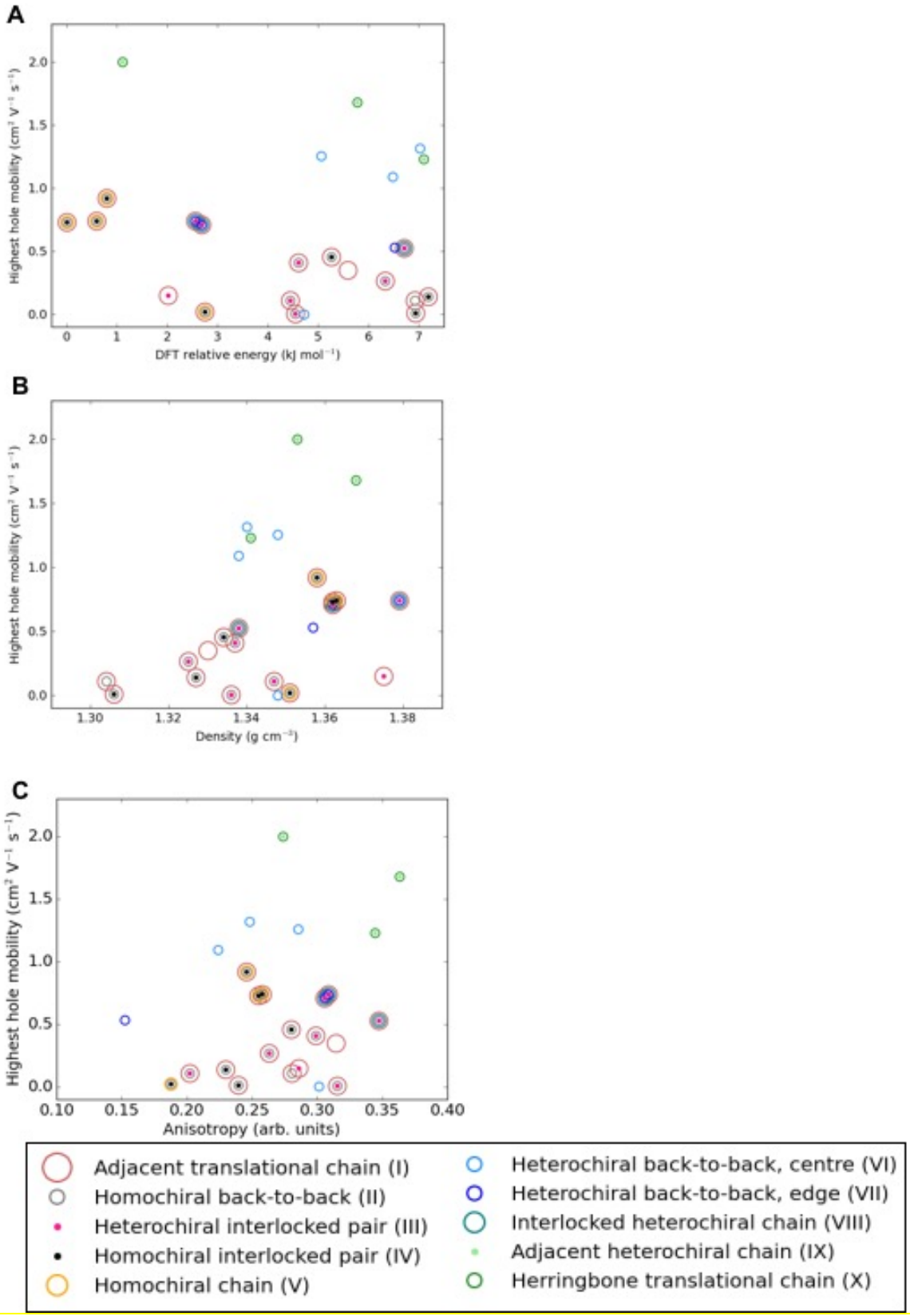

Figure S10: Hole mobility for the energetically low-lying [6]helicene polymorphs compared to (a) DFT relative energy, (b) density and (c) anisotropy of hole mobility. The data points are coloured according to the substructure type.

References

(1) M. J. Frisch, G. W. Trucks, H. B. Schlegel, G. E. Scuseria, M. A. Robb, J. R. Cheeseman, G. Scalmani, V. Barone, B. Mennucci, G. A. Petersson, H. Nakatsuji, M. Caricato, X. Li, H. P. Hratchian, A. F. Izmaylov, J. Bloino, G. Zheng, J. L. Sonnenberg, M. Hada, M. Ehara, K. Toyota, R. Fukuda, J. Hasegawa, M. Ishida, T. Nakajima, Y. Honda, O. Kitao, H. Nakai, T. Vreven, J. A. Montgomery Jr, J. E. Peralta, F. O. Ogliaro, M. J. Bearpark, J. Heyd, E. N. Brothers, K. N. Kudin, V. N. Staroverov, R. Kobayashi, J. Normand, K. Raghavachari, A. P. Rendell, J. C. Burant, S. S. Iyengar, J. Tomasi, M. Cossi, N. Rega, N. J. Millam, M. Klene, J. E. Knox, J. B. Cross, V. Bakken, C. Adamo, J. Jaramillo, R. Gomperts, R. E. Stratmann, O. Yazyev, A. J. Austin, R. Cammi, C. Pomelli, J. W. Ochterski, R. L. Martin, K. Morokuma, V. G. Zakrzewski, G. A. Voth, P. Salvador, J. J. Dannenberg, S. Dapprich, A. D. Daniels, Ã. D. N. Farkas, J. B. Foresman, J. V. Ortiz, J. Cioslowski and D. J. Fox, Gaussian09 (Revision D.01), Gaussian Inc., Wallingford, CT, USA, 2009.

(2) P. G. Karamertzanis and C. Pantelides, *J. Comput. Chem.*, 2005, **26**, 304–324

(3) P.G. Karamertzanis and C. Pantelides, *Mol, Phys,* 2007, **105**, 273.

(4) A. J. Stone, *J. Chem. Theory Comput.,* 2005, **1**, 1128-1132.

(5) A. J. Stone, GDMA (Version 2.2.02), 2005.

(6) S. Price, M. Leslie, G. Welch and M. Habgood, *Phys. Chem. Chem. Phys.,* 2010, **12**, 8478-8490.

(7) D. Williams, *J. Comput. Chem.*, 2001, **22**, 1154–1166.

(8) S. Ramdas, J. M. Thomas, M. E. Jordan and C. J. Eckhardt, *J. Phys. Chem.*, 1981, **85**, 2421–2425.

(9) J. A. Chisholm and S. Motherwell, *J. Appl. Cryst.*, 2005, **38**, 228-231.

(10) C. F. Macrae, I. J. Bruno, J. A. Chisholm, P. R. Edgington, P. McCabe, E. Pidcock, L. Rodriguez-Monge, R. Taylor, J. V. de Streek and P. A. Wood, *J. Appl. Cryst.*, 2008, **41**, 466-470.

(11) S. L. Childs, P. A. Wood, N. Rodríguez-Hornedo, L. S. Reddy, K. I. Hardcastle, *Cryst. Growth Des.,* 2009, **9**, 1869-1888.

(12) R. A. Marcus, *J. Chem. Phys.* 1956, **24**, 966-978.

(13) K. Sakanoue, M. Motoda, M. Sugimoto, S. Sakaki, *J. Phys. Chem. A* 1999, **103**, 5551.

(14) H. Houili, E. Tutiš, I. Batistić, L. Zuppiroli, *J. Appl. Phys.* 2006, **100**, 033702-13.

(15) D. J. Wolff, D. J. Grimwood, J. J. McKinnon, M. J. Turner, D. Jayatilaka, and M. A. Spackman, Crystal Explorer (Version 3.1), University of Western Australia, 2012.

(16) M. A. Spackman and D. Jayatilaka, *CrystEngComm* 2009, **11**, 19.
(17) M. A. Spackman, J. J. McKinnon, *CrystEngComm* 2002, **4**, 378.
(18) J. J. McKinnon, M. A. Spackman, A. S. Mitchell, *Acta Crystallogr. B*, 2004, **60**, 627–668.
(19) F. L. Hirshfeld, S. Sandler and G. M. J. Schmidt, *J. Chem. Soc.*, 1963, **0**, 2108-2119.
(20) R. Kuroda, *J. Chem. Soc. Perkin Trans. 2,* 1982, **7**, 789-794.
(21) P. T. Beurskens, G. Beurskens and T. E. M. van den Hark, *Cryst. Struct. Commun.* 1976, **5**, 241.
(22) G. Le Bas, A. Navaza, Y. Mauguen, and C. de Rango, *Cryst. Struct. Commun.* 1976, **5**, 357.
(23) E. D'Oria, P. G. Karamertzanis, and S. Price, *Cryst. Growth Des.* 2010, **10**, 1749-1756.
(24) M. Parschau and K.-H. Ernst, *Angew. Chem., Int. Ed.*, 2015, **127**, 14630-14634.
(25) R. H. Martin, *Angew. Chem., Int. Ed.*, **1974**, *13* (10), 649-660.